# Hydration Force in the Atomic Force Microscope: A Computational Study

Ruoya Ho,* Jian-Yang Yuan,[#] and Zhifeng Shao*

*Department of Molecular Physiology and Biological Physics, University of Virginia School of Medicine, Charlottesville, Virginia 22908 USA, and [#]Alberta Research Council, Edmonton, Alberta T6N-1E4, Canada

ABSTRACT    Using a hard sphere model and numerical calculations, the effect of the hydration force between a conical tip and a flat surface in the atomic force microscope (AFM) is examined. The numerical results show that the hydration force remains oscillatory, even down to a tip apex of a single water molecule, but its lateral extent is limited to a size of a few water molecules. In general, the contribution of the hydration force is relatively small, but, given the small imaging force (~0.1 nN) typically used for biological specimens, a layer of water molecules is likely to remain "bound" to the specimen surface. This water layer, between the tip and specimen, could act as a "lubricant" to reduce lateral force, and thus could be one of the reasons for the remarkably high resolution achieved with contact-mode AFM. To disrupt this layer, and to have a true tip-sample contact, a probe force of several nanonewtons would be required. The numerical results also show that the ultimate apex of the tip will determine the magnitude of the hydration force, but that the averaged hydration pressure is independent of the radius of curvature. This latter conclusion suggests that there should be no penalty for the use of sharper tips if hydration force is the dominant interaction between the tip and the specimen, which might be realizable under certain conditions. Furthermore, the calculated hydration energy near the specimen surface compares well with experimentally determined values with an atomic force microscope, providing further support to the validity of these calculations.

## INTRODUCTION

One of the most attractive features of the atomic force microscope (AFM) is the ability to image biological structures in aqueous solution (Shao et al., 1996; Hansma and Hoh, 1994; Engel et al., 1997; Bustamante et al., 1994). In fact, in the past several years, nanometer to subnanometer resolution has already been achieved with both soluble proteins (Mou et al., 1996a,b; McMaster et al., 1996; Müller and Engel, 1997) and membrane proteins (Yang et al., 1993a, b; Mou et al., 1995; Müller et al., 1995, 1996, 1997; Walz et al., 1996; Schabert et al., 1995; Czajkowsky et al., 1998) by the AFM in aqueous solutions. Despite these experimental advances, many aspects of AFM imaging of macromolecules are still poorly understood at present (Yang et al., 1996; Shao et al., 1996; Engel et al., 1997), and the ultimate limit of resolution has not yet been established either experimentally or theoretically (Yang et al., 1996). To have a reasonable understanding of the imaging process in solution, the interaction between the scanning tip and the surface of the macromolecule must be carefully considered; this is not only complex, but is also strongly dependent on the nature of the surfaces (Butt, 1991a,b, 1992; Shao et al., 1996).

From the imaging point of view, long-range interactions are probably less important, because these forces are likely to contribute only to a slowly varying background and to distribute over a large area on the specimen, resulting in small local deformations, provided that they are not very large in magnitude (Shao et al., 1996; Butt, 1991a,b; Müller and Engel, 1997). However, at short ranges, the hydration force (or solvation force in fluids other than water) is known to be important (Israelachvili and Pashley, 1983; Israelachvili, 1991; Cleveland et al., 1995; Grimson et al., 1980a,b; O'Shea and Welland, 1992; Grünewald and Helm, 1996; Meagher, 1992; O'Shea et al., 1994). It has been shown with two parallel plates in water that the pressure can easily exceed 100 atmospheric pressures at a distance below 2 nm (Israelachvili and Pashley, 1983; Israelachvili, 1991). Such a large pressure is due to the fact that solvent molecules tend to order themselves at the solvent-solid interface, and a fairly large energy is required to interrupt this order (Israelachvili and Pashley, 1983; Israelachvili, 1991; Grimson et al., 1980a,b; O'Shea and Welland, 1992; O'Shea et al., 1994; Luedtke and Landman, 1992; Bhushan et al., 1995; Israelachvili and Wennerström, 1996; Gelb and Lynden-Bell, 1993). Because of the finite size of the solvent molecules, the hydration force also tends to oscillate at a spatial period comparable to the size of the solvent molecule for two rigid surfaces (Israelachvili and Pashley, 1983; Israelachvili, 1991; Grimson et al., 1980a,b; O'Shea and Welland, 1992; O'Shea et al., 1994; Luedtke and Landman, 1992; Bhushan et al., 1995; Israelachvili and Wennerström, 1996; Gelb and Lynden-Bell, 1993). A large hydration force could have important implications for AFM imaging, because to "probe" the true surface of a macromolecule, the probe would have to break through the hydration "shell." Because most hydrated biological molecules are very soft (Urry, 1984, 1988; Barra et al., 1993; Linke et al., 1994; Suda et al., 1995), the magnitude of the force required to "break" the hydration shell could be critical. If the required force is too large, the structure below the hydration "shell"

could be deformed, resulting in a lower resolution. On the other hand, if the probe force is too small, the probe may not come into contact with the "true" sample surface, and the resolution would be lower. Therefore, it is both practically and conceptually important to have a good estimate of the magnitude of the hydration force at different tip shapes and sizes. Such knowledge will not only help us in the optimization of the imaging conditions, but may also be useful for the design of the "ultimate" AFM tip for high-resolution imaging.

Although the hydration force between flat parallel or macroscopically curved surfaces has been extensively studied (Israelachvili and Pashley, 1983; Israelachvili, 1991; Grimson et al., 1980a,b; Luedtke and Landman, 1992; Bhushan et al., 1995), detailed studies in the context of an AFM tip and a flat surface (specimen) have been rather limited (Butt, 1991b; Cleveland et al., 1995; Gelb and Lynden-Bell, 1993; Koga and Zeng, 1997; O'Shea and Welland, 1992; O'Shea et al., 1994). Experimentally, the magnitude of the hydration force could only be inferred because of the presence of other longer range forces (Butt, 1991b), although the oscillatory behavior was recently detected in the AFM (Cleveland, et al., 1995). However, because of the lack of control over the shape of the AFM tip in the experiments, it is difficult to establish a direct connection between the hydration force and the tip geometry. For example, it is not clear how far the hydration force extends laterally and whether the surface beyond the very end of the tip could contribute substantially to the hydration force. From this point of view, a theoretical investigation of these aspects of the hydration force can still contribute significantly to our understanding of the imaging process in the AFM.

In this paper, using a hard sphere model with the Ornstein-Zernike direct correlation function (Hansen and McDonald, 1976; Grimson et al., 1980a,b; Press et al., 1986), we consider the hydration force between a flat specimen surface and a conically shaped tip with a spherical apex that is close to the real AFM tip and is not subject to the limitations of a previous study, in which the tip was assumed to be a small sphere and an approximation had to be used to model the solvation force (Gelb and Lynden-Bell, 1993). Unlike atomic simulations in which only a very small tip could be examined (Patrick and Lynden-Bell, 1997), a tip size closer to that inferred from experimental results can be accommodated with this method, although the temporal aspect of the hydration force could not be addressed, which has been described recently with a "single atom tip" on a hydrophobic surface (Koga and Zeng, 1997). Based on the numerical solutions, we show that, at low imaging forces, a layer of water molecules is most likely to remain between the tip and the specimen, perhaps providing the necessary "lubrication" that could reduce the lateral friction during scanning, and explaining, in part, how contact mode imaging has achieved high resolution (Müller et al. 1995, 1996; Engel et al., 1997; Mou et al., 1995, 1996a,b; Czajkowsky et al., 1998; Yang et al., 1993a, b). Our results also show

that the hydration force is nearly completely dominated by the apex. The magnitude of the hydration force increases linearly with the radius of curvature at the apex, and for a spherical apex, the hydration force scales nearly exactly with the radius. Furthermore, the lateral extent of the hydration force is proportional to the square root of the radius of the apex, indicating that the hydration effect is rather localized.

## THEORY AND METHOD OF COMPUTATION

Hydration force can be described by using a hard sphere model (Grimson et al., 1980a,b), where the solvent molecules are approximated as a noncompressible solid spheres. This commonly used treatment drastically simplifies the model as well as the calculations. In essence, this is a continuum model in which the density fluctuations are calculated with the given boundary conditions (Hansen and McDonald, 1976; Grimson et al., 1980a,b). Although this model could not include other effects such as solubilized ions and molecular deformations, or address dynamic aspects of the hydration force, which can be important at atomic scales (Patrick and Lynden-Bell, 1997; Koga and Zeng, 1997), the inclusion of these effects is not essential, because the purpose of this study is only an estimation of the hydration force.

For a small density fluctuation $\delta\rho(\mathbf{r})$, the change in thermodynamic potential $\Delta\Omega(\delta\rho(\mathbf{r}))$ can be written as

$$\Delta\Omega[\delta\rho(\mathbf{r})]$$
$$= \frac{1}{2\beta\rho_0}\left[\int \delta\rho^2(\mathbf{r})d\mathbf{r} - \rho_0\int \delta\rho(\mathbf{r})c(\mathbf{r} - \mathbf{r}')\delta\rho(\mathbf{r}')d\mathbf{r}\, d\mathbf{r}'\right]$$
$$(1)$$

where $\beta = (kT)^{-1}$, $\rho_0$ is the bulk liquid density, $\rho(\mathbf{r})$ is the density distribution, and $\delta\rho(\mathbf{r}) = \rho(\mathbf{r}) - \rho_0$. $c(\mathbf{r})$ is the Ornstein-Zernike direct correlation function, and each of the integrals is over the entire space. For the hard sphere model, $c(\mathbf{r})$ can be written as (Hansen and McDonald, 1976; Grimson et al., 1980a)

$$c(\mathbf{r}) = -\theta(\sigma - r)\left[\lambda_1 + 6\eta\lambda_2\left(\frac{r}{\sigma}\right) + \frac{1}{2}\eta\lambda_1\left(\frac{r}{\sigma}\right)^3\right] \quad (2)$$

where

$$\eta = \pi\sigma^3\rho_0/6$$
$$\lambda_1 = (1 + 2\eta)^2/(1 - \eta)^4$$
$$\lambda_2 = -(1 + \eta/2)^2/(1 - \eta)^4$$
$$\theta(\sigma - r) = \begin{cases} 1 & r \le \sigma \\ 0 & r > \sigma \end{cases} \quad (3)$$

where $\sigma$ is the molecular size (diameter). Under any given condition, $\delta\rho(\mathbf{r})$ can be found by making $\Delta\Omega(\delta\rho(\mathbf{r}))$ stationary. Following the approach of Grimson et al. (1980a,b), the

density distribution can be written as

$$\rho(\mathbf{r}) - \rho_0 \int_v d\mathbf{r}' \, \rho(\mathbf{r}')c(\mathbf{r} - \mathbf{r}') = A \qquad (4)$$

where $A = \sigma^3\rho_0[1 - \sigma^3\rho_0\hat{c}(0)]$, $c(\hat{\mathbf{k}}) = \int d\mathbf{r} \, c(\mathbf{r})e^{-i\mathbf{kr}}$ and $\hat{c}(0) = -4\pi[(1 + 0.25\eta)\lambda_1 + 4.5\eta\lambda_2]/3$. $A$ is a constant depending on the experimental conditions. The integration is over the entire liquid volume, because in the solid volume, the density distribution will not change. The hydration force at the tip-sample distance $D$ can then be calculated as (Grimson et al., 1980a,b)

$$f = -\frac{\partial\Delta\Omega}{\partial\delta D} \qquad (5)$$

To calculate the hydration force, $\Delta\Omega$ must be calculated for each $D$ value within the distance range of interest.

In the process of obtaining numerical solutions, the continuum space must be converted to a discrete lattice. For a three-dimensional, uniformly partitioned lattice, Eq. 4 becomes

$$\rho(\mathbf{r}_i) - \sum_j \rho_0\rho(\mathbf{r}_i)c(\mathbf{r}_i - \mathbf{r}_j)\tau = A \qquad (6)$$

which can be rewritten in a more convenient form:

$$\sum_j \{\delta_{ij} - \tau\rho_0 c(\mathbf{r}_i - \mathbf{r}_j)\}\rho(\mathbf{r}_j) = A \qquad (7)$$

where $\tau$ is the volume of each voxel (a constant). The above equation can now be expressed in a matrix form:

$$M_{ij}X_j = A \qquad (8)$$

where

$$\begin{cases} M_{ij} = \delta_{ij} - \rho_0 c(\mathbf{r}_i - \mathbf{r}_j)\tau \\ \quad\quad X_j = \rho(\mathbf{r}_j) \end{cases}$$

which can be solved by the standard method (Press et al., 1986), and the problem of solving Eq. 4 now becomes a problem of matrix inversion.

For an acceptable accuracy, the size of each voxel should be at least smaller than the volume of the solvent molecule. Therefore, even for a calculation of $20 \times 20 \times 20$ molecules, a direct calculation in three dimensions will still require a significant amount of computer memory. However, because the AFM tip can be reasonably modeled by a conical shape, the calculation can be simplified greatly by taking advantage of the rotational symmetry. In this case, the calculation becomes two dimensional, and Eq. 4 can be written as

$$\rho(r, z) - \rho_0 \int_0^R r' \, dr' \int_0^Z dz' \, c(r, r', z - z')\rho(r', z') = A$$
$$(9)$$

where

$$c(r, r', z - z')$$
$$= \int_0^{2\pi} d\phi \, c(\sqrt{r^2 + r'^2 - 2rr' \cos(\phi) + (z - z')^2}) \quad (10)$$

Because of the effect of $\theta(\sigma - r)$ in $c(\mathbf{r})$, the integration range of $\phi$ is simply $[\phi_{min}, \phi_{max}]$, instead of $[0, 2\pi]$, where

$$\phi_{max} = \left|\cos^{-1}\left(\frac{(z - z')^2 + r^2 + r'^2 - \sigma^2}{2rr'}\right)\right|$$

$$\phi_{min} = -\phi_{max} \qquad (11)$$

It should be noted that the voxel volume $\tau$ as a function of $r$ must be used in the calculation, if the same dimensions in both $r$ and $z$ directions are used for the lattice. With this reduction from three dimensions to two dimensions, an effective size of $50 \times 25$ molecules can be reasonably accommodated by a supercomputer, such as the Cray C90, for a lattice size of $0.25\sigma$ ($200 \times 100$ lattice points). For lattices greater than this size, the required computer memory becomes too large to be practical for computation facilities we have access to. Therefore, all of our calculations are confined to a size smaller than $50\sigma \times 25\sigma$ ($200 \times 100$ lattice points), which is equivalent to $100,000–200,000$ molecules in three dimensions, depending on the geometry of the boundaries.

To validate our computational model, we first calculated the hydration force between two parallel surfaces, which has been studied previously (Grimson et al., 1980a,b). The liquid bulk density was set to $\sigma^3\rho_0 = 0.6$, which is the same as that used by Grimson et al. (1980a,b). The diameter of the water molecule, $\sigma$, for this density, is $\sim2.6$ Å, which is in the midrange of the values used in other studies (Israelachvili, 1991; Cantor and Schimmel, 1980; Koga and Zeng, 1997; Cleveland et al., 1995). To ensure the conservation of solvent molecules, the system shown in Fig. 1 $a$ was considered, where a hard disk with a radius of $10\sigma$ and a thickness of $1\sigma$ is placed close to the bottom wall of a chamber $15\sigma \times 15\sigma$ ($30\sigma$ in diameter) in size, filled with water. As shown in Fig. 1 $b$, the calculated pressure is nearly identical for different chamber sizes ($15\sigma \times 15\sigma$, $15\sigma \times 25\sigma$, and $25\sigma \times 15\sigma$), indicating that the effects from the side and the top of the chamber are negligible. Even in the extreme case of allowing no space between the edge of the disk and the side wall (still maintaining a constant number of water molecules), the difference in the calculated pressure is still very small. Therefore, in all following calculations, a distance of $5\sigma$ is allowed between the edge of the disk (or a tip) and the wall of the chamber in the radial direction. These results are identical, as they should be, to those obtained by Grimson et al. (1980a).

To improve the efficiency of the calculation, the effect of lattice size relative to the size of the solvent molecule was examined. As shown in Fig. 2, the density profiles for lattice
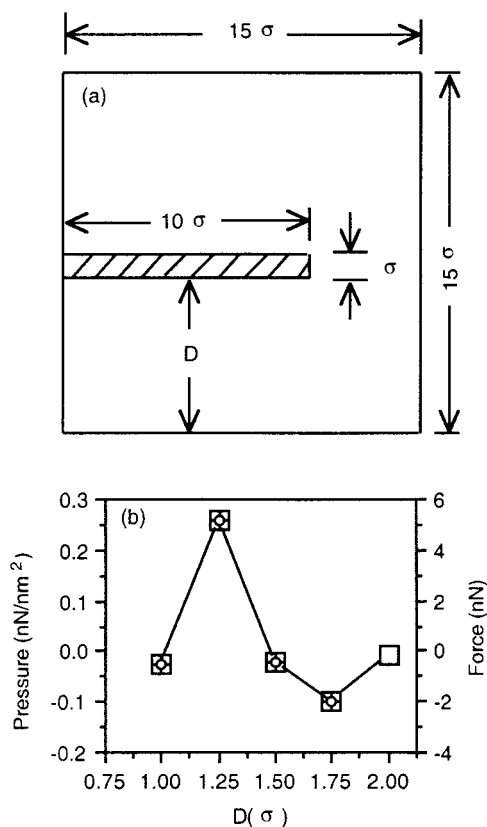
FIGURE 1  (a) Schematic illustration of the model system used to validate the numerical method. $\sigma$ is the diameter of the solvent molecule. The flat disk has a radius of $10\sigma$ and a thickness of $1\sigma$. The total number of solvent molecules is conserved in the calculation (when the disk is moved toward the specimen, i.e., the bottom wall of the chamber). (b) The calculated hydration pressures for three different chamber sizes. $\square$, $15\sigma \times 15\sigma$; $+$, $25\sigma \times 15\sigma$; $\bigcirc$, $15\sigma \times 25\sigma$. In these calculations, a lattice size of $0.25\sigma$ was used. The results are identical, demonstrating that the effect of the side and the top of the chamber is negligible.

sizes $0.1\sigma$ and $0.125\sigma$ are virtually identical, and even for the case of $0.25\sigma$, the results are still reasonably close to those of smaller lattice spacing. The slight shift of the curve
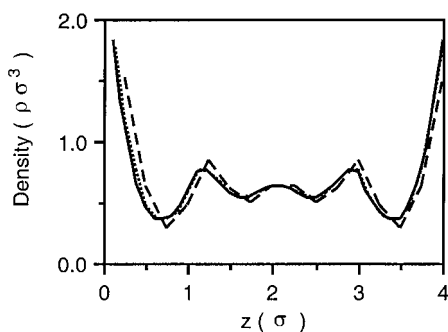
is probably related to the "rough" surface of hard spheres due to the coarse lattice spacing. Therefore, throughout this study, a $0.25\sigma$ lattice size is used in all calculations. The maximum error in the density profile, as estimated from these trial calculations, is less than 20% (standard deviation). The error of the calculated hydration force should be smaller, because the hydration force is calculated by integrating the density changes over the entire volume, so that most of the error in density profiles should be averaged out.

The calculated hydration force (per nm$^2$) for a flat disk and a flat surface at a lattice size of $0.25\sigma$ is shown in Fig. 3. The oscillatory behavior of the hydration force is identical to that obtained by Grimson et al. (1980a,b). However, the peak value of the calculated hydration force is only 18% of that derived from measurements of two macroscopically curved surfaces (Israelachvili and Pashley, 1983; Israelachvili, 1991), but is consistent with other theoretical calculations (Henderson and Lozada-Cassou, 1986; Grimson et al, 1980a,b). This discrepancy is most likely due to the particular experimental method used to measure the hydration force, in which an overestimate of the peak value is considered to be understood (Israelachvili, 1991). Therefore, these test calculations show that the method we adopted is a reasonable approximation and the computational method used is valid. These results also provide a necessary control for the calculation of the hydration force under the more complex geometry of an AFM tip.

## RESULTS AND DISCUSSION

The AFM tip is modeled as a conical body with a spherical apex. The conical angle is set at 35°, which is typical for most commercial cantilevers (Albrecht et al., 1990). Because the hydration force is a short-range interaction, the effect of the base of the tip should be minimal (see below). In all calculations, the upper boundary of the chamber is at least $10\sigma$ from the top of the tip. We should indicate that this configuration, although much smaller than the physical



FIGURE 2  Density profiles calculated for three different lattice sizes, $0.1\sigma$ (= $\sigma/10$, ——), $0.125\sigma$ (= $\sigma/8$, · · · ·), $0.25\sigma$ (= $\sigma/4$, – – –), for a system $12\sigma \times 4\sigma$ in size (parallel plates). Clearly, even for $\sigma/4$, the accuracy of the calculation is still acceptable. The small deviation from the profiles of smaller lattices is its inability to accurately describe the spherical shape of the hypothetical solvent molecules. See text for more details.
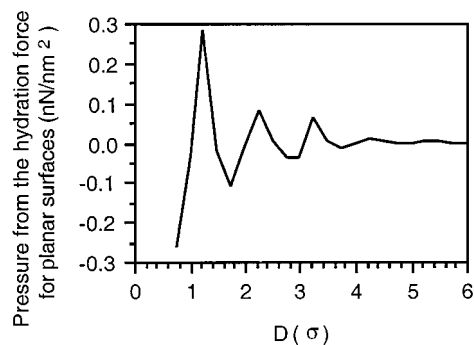


FIGURE 3  The calculated hydration force per unit area for a flat disk and a flat specimen surface at a step size of $0.25\sigma$. The well-known oscillatory behavior is reproduced, and the quasiperiodicity of the oscillation is correlated to the size of the solvent molecule. This is identical to the results obtained by Grimson et al. (1980a), demonstrating the validity of the numerical approach developed here.

size of an actual AFM tip, is closer to the experimental conditions, in which the entire cantilever is submerged in solution. To evaluate the dependence of the hydration force on the detailed geometry of the tip, we have considered three similar configurations. In tip shape 1, the apex has a radius of curvature of $15\sigma$ (3.9 nm), whereas in shape 2, this radius is reduced to $5\sigma$ (1.3 nm), and in shape 3, an ideal tip is considered, where the apex is simply a single molecule ($1\sigma$), which, although not practical, is helpful for our understanding of the trend of the hydration force when the apex of the tip is continuously reduced. Based on experimental results, the best high-resolution tips should have an apex in the range of 1–2 nm (Mou et al., 1996a; Müller et al., 1995), which is very close to the size of shape 2 (1.3 nm). The calculated hydration forces for these three cases are shown in Fig. 4. It is seen that all three tips have a very similar, oscillatory behavior, but the magnitude of the hydration force varies by a factor of ~27 between shape 3 and shape 1. For the sharpest tip, the hydration force is almost negligible, which is expected, because the conical shape of the tip should easily allow the "trapped" water molecules to be displaced, without an expensive energy cost. The magnitude of the hydration force in this case is actually close to that of a single atom, recently considered by Koga and Zeng (1997). But, for more practical tips of nanometer size, the magnitude of the hydration force is no longer very small and, in fact, becomes measurable. This was not expected, because even for the largest tip considered (3.9 nm), one might think that the conical surface of the tip should still allow water molecules to leave easily. It is also a surprise to see the profound oscillatory behavior of the hydration force under these conditions, because one would expect that the oscillation should be averaged out, because the conical tip surface crosses many water layers. Apparently, because of the nonadditive nature of the hydration force, the conical tip cannot be treated as many flat rings at various distances
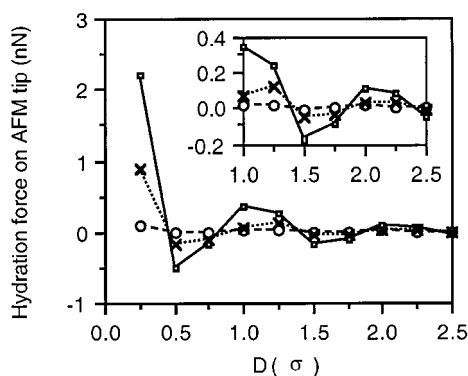
with each being regarded as a planar surface. Interestingly, at the tip-sample distance of just one layer of water molecules, the hydration force is already in the subnanonewton range for both shapes 1 and 2. Because a probe force of less than 0.5 nN is often required to attain high-resolution images of biological specimens (Shao et al., 1996; Engel et al., 1997), this result seems to suggest that at least one layer of water molecules might remain "bound" to the sample surface during imaging, which could provide a "lubricating" effect. This is because the ordering of water molecules at the surface is dynamic in nature, which could reduce the lateral force imposed on the specimen by the scanning probe. This may also partially explain why contact mode AFM imaging, when operated at very small forces, has produced remarkable high-resolution images of a number of biological specimens (Shao et al., 1996; Engel et al., 1997). The force required to have a true contact (at $D = 0$ nm) between the tip and the specimen appears to be too great to be practical for biological imaging, where the deformation of the specimen becomes a more serious problem. It may be noted that, for atomic resolution imaging of hard surfaces, such as mica, nanonewton probe forces were known to improve the image quality (Czajkowsky, unpublished observation). Perhaps, in this case, the last water layer is penetrated and the true surface structure is probed by the tip. Obviously, the surface water layer could also impose a practical resolution limit of ~0.5 nm, which is actually quite close to the highest resolution achieved to date with biological specimens (Czajkowsky et al., 1998; Müller et al., 1995; Mou et al., 1995).

From Fig. 4, one should have noticed that the hydration force peaks at tip-sample distances of integral multiples of the molecular size. This suggests that the apex of the tip should dominate the hydration force measurements. To examine this issue, we have compared the calculated hydration force for two tips. Each has a spherical apex of $5\sigma$, but they differ in shape: one has a 35° semiangle (shape 2), and the other is cylindrical (Fig. 5 $a$). As expected, the hydration force is identical for the two tips (see Fig. 5 $b$), demonstrating that the very end of the tip is far more important than the detailed shape of the tip body. A comparison of the hydration force for shape 3 (Fig. 4) and that of a single atom (Koga and Zeng, 1997) also supports this conclusion. Therefore, as far as the hydration force is concerned, one need only consider the very apex of the tip, which is consistent with the short-range nature of the hydration force. This result clearly shows that if small asperities are present on the otherwise smooth surface of the tip, these asperities will be the primary contributor to the hydration force.

To date, an important experimental assessment of the hydration effect by AFM is that of Cleveland et al. (1995), in which the hydration force between a tip and crystal surfaces (calcite or barite) was examined by a statistical analysis of the cantilever fluctuations. Although the hydration force could not be measured directly with this technique, the energy required to move the tip between the hydration layers was obtained, which was on the order of $5 \times 10^{-21}$ J, only slightly above the thermal energy, $4 \times$



FIGURE 4   The calculated hydration force for the three AFM tip shapes described in the text. (*Inset*) Details for the region some distance away from the surface. The solid line with squares, the dotted line with crosses, and the dashed line with circles indicate the hydration force for tip shapes 1, 2, and 3, respectively. Even for these small tips, the oscillatory behavior is still profound, and the peak positions still correspond to the size of the water molecule, although they are slightly shifted when compared with that of flat surfaces. The three curves scale precisely.
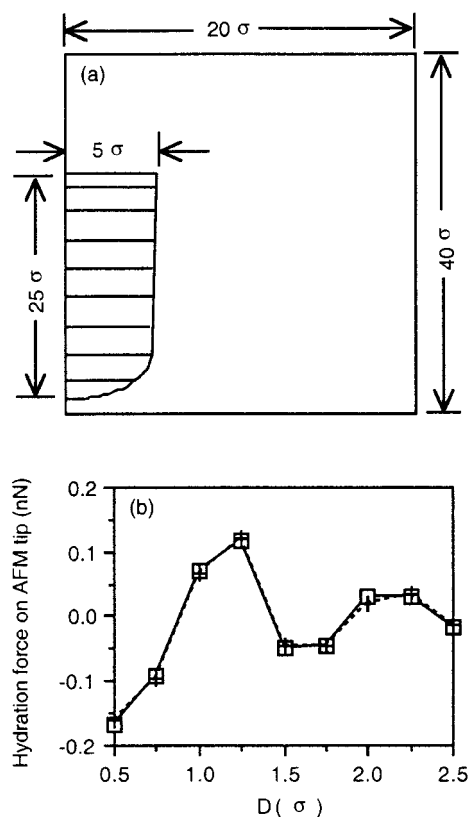
FIGURE 5  A comparison of two tips with the same spherical apex ($R = 5\sigma$), one with a conical shape and the other with a straight cylinder ($a$). The hydration force for these two tips is identical. The solid line with squares is the hydration force for tip shape 2, used in Fig. 4 (conical body), and the dashed line with pluses is that of the cylindrical tip. Therefore the hydration force is completely dominated by the apex of the tip. Thus a small asperity on a large, smooth tip surface should exhibit a hydration force as if the tip were a long needle the size of the asperity.

$10^{-21}$ J, at room temperature (Cleveland et al., 1995), with 1.5–3 Å between the peak positions. The calculated hydration force in the present study can be easily converted to that of energy by taking an integration from infinity (see Fig. 6). The energy difference between $1\sigma$ and $1.5\sigma$ for shape 2 is $\sim 12 \times 10^{-21}$ J. This is within 2 times the experimental value, which is a surprise, considering the crude model used in this study and the lack of control of the experimental conditions. Even though the nominal size of the tip used in the experiment was nearly 60 nm, as indicated by the authors (Cleveland et al., 1995), it is almost certain that the measured hydration effect was due to a small asperity of nanometer size on the blunt tip, because the rest of the tip should not contribute significantly to the hydration force, as already discussed above. Such a tip geometry was already suggested to be responsible for high-resolution imaging by a number of investigators (Shao et al., 1996; Yang et al., 1996; Engel et al., 1997; Radmacher et al., 1992).

We may further define an effective tip size as the area enclosed by a single water layer when the tip is in contact with the sample surface. The effective tip size can be estimated as $\pi(2R\sigma - \sigma^2)$ ($R$ is the radius of the apex of the
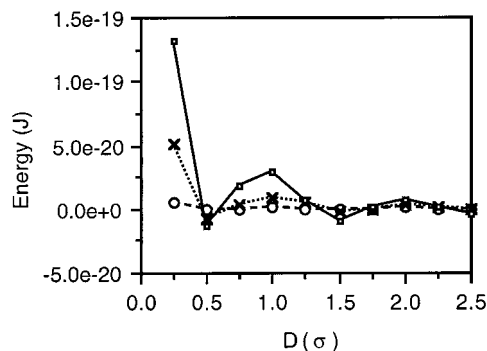


FIGURE 6  The corresponding hydration energy calculated from the hydration force curves shown in Fig. 4. The solid line with squares, the dotted line with crosses, and the dashed line with circles indicate the hydration energies of tip shapes 1, 2, and 3, respectively. It is seen that the magnitude for shape 2 at $D = 1\sigma$ is very close to that determined by experiments (Cleveland et al., 1995). See text for more discussion.

tip; this is the tip cross-sectional area cut by a plane from the surface at a distance of $\sigma$). We found that the estimated "hydration pressure" (hydration force divided by the effective tip size) on the tip is almost the same for all three tips used in Fig. 4 (Fig. 7). This is an interesting finding, because, as far as the hydration force is concerned, the penalty for a very sharp tip may not be significant, i.e., the hydration pressure does not increase. As already indicated previously (Shao et al., 1996; Yang et al., 1996), it is the tip pressure that must be reduced, rather than the total force. If $\sigma \ll R$, it can be approximated as $2\pi R\sigma$. Because the "hydration pressure" is a constant for all tips with a spherical apex, the total hydration force increases linearly with the radius of the curvature, $R$, of the tip apex, because for the same solvent, $\sigma$ is always the same. We should point out that the pressure between two planar surfaces at comparable distances is much greater than the results shown in Fig. 7,
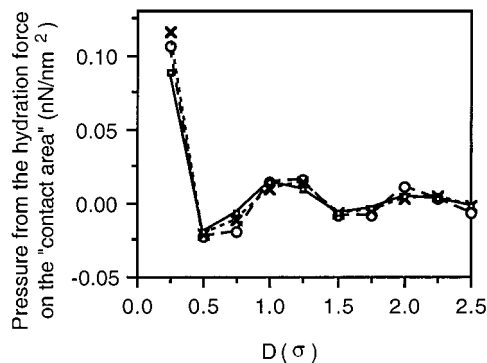


FIGURE 7  If an "effective contact area" is defined as the area intersected by the surface at $1\sigma$ from the specimen when the end of the tip is in touch with the specimen, the "hydration pressure" is found to be the same for all three tip shapes used in Fig. 4 (solid line with squares, dotted line with crosses, and dashed line with circles for tip shapes 1, 2, and 3, respectively). Therefore, a smaller tip will not increase the contact pressure if the hydration force dominates the interaction in imaging. It is noted that the pressure calculated here is much smaller than that of two parallel plates of the same size.

indicating that one cannot simply scale down the results from planar surfaces to estimate the hydration force of other geometrical shapes. If these results could be generalized, perhaps one may conclude that the characteristic pressure is determined solely by the geometric shape of the apex. Simply increasing the dimensions in proportion will not alter this characteristic pressure. For the spherical apex considered in this study, one can easily establish an empirical formula for the estimation of the hydration force, which should depend on the distance between the tip and the specimen. At $1\sigma$ (one layer of water remaining), the hydration force may be estimated as

$$F \text{ (nN)} \approx 0.082 \times R \text{ (nm)} \qquad R \gg \sigma \qquad (12)$$

Here we have assumed that $R$, the radius of curvature at the apex, is greater than the size of the water molecule. Otherwise, a small correction will be required:

$$F \text{ (nN)} \approx 0.082 \times [R \text{ (nm)} - \sigma \text{ (nm)}/2] \qquad (13)$$

Another important issue that needs to be addressed is the lateral extent of the hydration force on the specimen surface, which is directly relevant to the achievable lateral resolution for AFM imaging, when under certain conditions, the hydration force is the dominating interaction. As discussed by Grimson et al. (1980a,b), the surface pressure on a flat solid surface at the solid-liquid interface is dependent on the liquid molecular density distribution on the surface, and can be evaluated by the following equation:

$$p = \frac{\rho(\mathbf{r})^2 - \rho(\infty)^2}{2\beta\rho_0} \qquad (14)$$

Because it appears most appropriate for imaging in solution when the tip is about one molecular layer from the sample surface, we have calculated the surface pressure for all three tips used in Fig. 4 under this condition. We found that the radius of the area that contains 50% of the total hydration force is $1.6\sigma$, $0.9\sigma$, and $0.4\sigma$, respectively, for $R = 15\sigma$, $5\sigma$, and $1\sigma$. If we define the "lateral spread" of the hydration force, $\Delta/\sigma$, as twice this value, it is related linearly to the square root of the radius of curvature of the apex: $\Delta/\sigma = 0.82(R/\sigma)^{1/2}$. This relationship was obtained by a least-squares fitting of the numerical results. Therefore, the "spread" improves slowly with the reduction of the tip size. Nonetheless, even for the largest tip considered here, $R = 15\sigma$, the lateral range of the hydration force is still very small, only about three water molecules ($\sim$1 nm). These results indicate that the hydration force remains rather localized, consistent with its short interaction range.

In summary, we have shown that the simple numerical model used to calculate the hydration force for a conical tip in front of a nondeformable flat surface can be qualitatively compared with the experimental results obtained with an AFM (Cleveland et al., 1995). With this model, we show that the hydration force remains oscillatory, even for a tip not much greater than a single water molecule. With the several tip geometries considered, it is established that the hydration force is completely dominated by the apex of the tip. A simple empirical formula is proposed for the estimation of the hydration force for a given tip with a spherical apex, and the lateral spread of the hydration force on the specimen surface is comparable to the "effective contact area," which decreases with the square root of the tip radius. The magnitude of the hydration force for a practical tip size, $\sim$1 nm, seems to suggest that at least one layer of water should remain largely "bound," which may provide a "lubricating" effect during imaging, a possible explanation for the high-resolution images obtained with contact-mode AFM. In practical terms, the hydration force imposes only a minor effect in AFM imaging in solution, and can be largely neglected for routine experiments. However, for most delicate specimens or very high-resolution imaging, its effect may become significant. Thus very sharp asperities on a blunt tip surface should be beneficial to the reduction of the magnitude of the hydration force and, at the same time, provide the necessary conditions for high-resolution imaging.

## REFERENCES

Albrecht, T. R., S. Akamine, T. E. Carver, and C. F. Quate. 1990. Microfabrication of cantilever styli for the atomic force microscope. *J. Vac. Sci. Technol. A.* 8:3386–3396.

Barra, J. G., R. L. Armentano, J. Levenson, E. I. C. Fisher, R. H. Pichel, and A. Simon. 1993. Assessment of smooth muscle contribution to descending theoracic aortic elastic mechanics in conscious dogs. *Circ. Res.* 73:1040–1050.

Bhushan, B., J. N. Israelachvili, and U. Landman. 1995. Nanotribology: friction, wear and lubrication at the atomic scale. *Nature.* 374:607–616.

Bustamante, C., D. Erie, and D. Keller. 1994. Biochemical and structural applications of scanning force microscopy. *Curr. Opin. Struct. Biol.* 4:750–760.

Butt, H.-J. 1991a. Electrostatic interaction in atomic force microscopy. *Biophys. J.* 63:578–582.

Butt, H.-J. 1991b. Measuring electrostatic, van der Waals, and hydration force in electrolyte solutions with an atomic force microscope. *Biophys. J.* 60:1438–1444.

Butt, H.-J., 1992. Measuring local surface charge densities in electrolyte solutions with a scanning force microscope. *Biophys. J.* 63:578–582.

Cantor, C. R. and P. R. Schimmel. 1980. Biophysical Chemistry, Part II: Techniques for the Study of Biological Structure and Function. W. H. Freeman and Company, New York.

Cleveland, J. P., T. E. Schaffer, and P. K. Hansma. 1995. Probing oscillatory hydration potentials using thermal-mechanical noise in an atomic-force microscope. *Phys. Rev. B.* 52:R8692–R8695.

Czajkowsky, D. M., S. Sheng, and Z. Shao. 1998. Staphylococcal $\alpha$-hemolysin can form hexamers in phospholipid bilayers. *J. Mol. Biol.* 276:325–330.

Engel, A., C. A. Schoenenberger, and D. J. Müller. 1997. High resolution imaging of native biological sample surfaces using scanning probe microscopy. *Curr. Opin. Struct. Biol.* 7:279–284.

Gelb, L. D., and R. M. Lynden-Bell. 1993. Force oscillations and liquid structure in simulations of an atomic force microscope tip in a liquid. *Chem. Phys. Lett.* 211:328–332.

Grimson, M. J., G. Rickayzen, and P. Richmond. 1980a. Short range solvation forces in fluids. I. General formalism and hard particle fluids. *Mol. Phys.* 39:61–73.

Grimson, M. J., G. Rickayzen, and P. Richmond. 1980b. Solvation force in fluids. II. Ornstein-Zernike and Percus-Yevick temperature dependent fluids. *Mol. Phys.* 39:1455–1462.

Grünewald, T., and C. A. Helm. 1996. Computer-controlled experiments in the surface forces apparatus with a CCD-spectrograph. *Langmuir.* 12: 3885–3890.

Hansen, J. P., and I. R. McDonald. 1976. Theory of Simple Liquids. Academic Press, London.

Hansma, H. G., and J. Hoh. 1994. Biomolecular imaging with the atomic force microscope. *Annu. Rev. Biophys. Biomol. Struct.* 23:115–128.

Henderson, D., and M. Lozada-Cassou. 1986. A simple theory for the force between spheres immersed in a fluid. *J. Colloid Interface Sci.* 114: 180–183.

Israelachvili, J. N. 1991. Intermolecular and Surface Forces, 2nd Ed. Academic Press, San Diego.

Israelachvili, J. N., and R. M. Pashley. 1983. Molecular layering of water at surfaces and origin of repulsive hydration forces. *Nature.* 306: 249–250.

Israelachvili, J. N., and H. Wennerström. 1996. Role of hydration and water structure in biological and colloidal interactions. *Nature.* 379: 219–225.

Koga, K., and X. C. Zeng. 1997. Scanning motions of an atomic force microscope tip in water. *Phys. Rev. Lett.* 79:853–856.

Linke, W. A., V. I. Popov, and G. Pollack. 1994. Passive and active tension in single cardiac myofibrils. *Biophys. J.* 67:782–792.

Luedtke, W. D., and U. Landman. 1992. Solid and liquid junctions. *Comp. Mater. Sci.* 1:1–24.

McMaster, T. J., M. J. Miles, and A. E. Walsby. 1996. Direct observation of protein secondary structure in gas vesicles by atomic force microscopy. *Biophys. J.* 70:2432–2436.

Meagher, L. 1992. Direct measurement of forces between silica surfaces in aqueous $CaCl_2$ solutions using an atomic force microscope. *J. Colloid Interface Sci.* 152:293–295.

Mou, J., D. M. Czajkowsky, S. Sheng, R. Ho, and Z. Shao. 1996a. High resolution surface structure of *E. coli* GroES oligomer by atomic force microscopy. *FEBS Lett.* 381:161–164.

Mou, J., S. Sheng, R. Ho, and Z. Shao. 1996b. Chaperonins GroEL and GroES: views from atomic force microscopy. *Biophys. J.* 71:2213–2221.

Mou, J., J. Yang, and Z. Shao. 1995. Atomic force microscopy of cholera toxin B. oligomer bound to bilayers of biologically relevant lipids. *J. Mol. Biol.* 298:507–512.

Müller, D. J., M. Baumeister, and A. Engel. 1996. Conformational change of the hexagonally packed intermediate layer of *Deinococcus radiodurans* monitored by atomic force microscopy. *J. Bacteriol.* 178: 3025–3030.

Müller, D. J., G. Büldt, and A. Engel. 1995. Force-induced conformational change of bacteriohodopsin. *J. Mol. Biol.* 249:239–243.

Müller, D. J., and A. Engel. 1997. The height of biomolecules measured with the atomic force microscope depends on electrostatic interactions. *Biophys. J.* 73:1633–1644.

Müller, D. J., A. Engel, J. L. Carrascosa, and M. Vélez. 1997. The bacteriophage phi-29 head-tail connector imaged at high resolution with the atomic force microscope in buffer solution. *EMBO J.* 16:2547–2553.

O'Shea, S. J., and M. E. Welland. 1992. Solvation force near a graphite surface measured with an atomic force microscope. *Appl. Phys. Lett.* 60:2356–2358.

O'Shea, S. J., M. E. Welland, and J. B. Pethica. 1994. Atomic force microscopy of local compliance at solid-liquid interfaces. *Chem. Phys. Lett.* 223:336–340.

Patrick, D. L., and R. M. Lynden-Bell. 1997. Atomic simulations of fluid structure and solvation forces in atomic force microscopy. *Surface Sci.* 380:224–244.

Press, W. H., B. P. Flanney, S. A. Teukolsky, and W. T. Vetterling. 1986. Numerical Recipes. Cambridge University Press, New York.

Radmacher, M., R. W. Tillmann, M. Fritz, and H. F. Gaub. 1992. From molecules to cells: imaging soft samples with the atomic force microscope. *Science.* 257:1900–1905.

Schabert, F. A., C. Henn, and A. Engel. 1995. Native *Escherichia coli* OmpF porin surface probed by atomic force microscopy. *Science.* 268: 92–94.

Shao, Z., J. Mou, D. M. Czajkowsky, J. Yang, and J.-Y. Yuan. 1996. Biological atomic force microscopy: what is achieved and what is needed. *Adv. Phys.* 45:1–86.

Suda, H., M. Sugimoto, M. Chiba, and C. Uermura. 1995. Direct measurements for elasticity of myosin head. *Biochem. Biophys. Res. Commun.* 211:219–225.

Urry, D. W. 1984. Protein elasticity based on conformations of sequential polypeptides: the biological elastic fibre. *J. Protein Chem.* 3:403–436.

Urry, D. W. 1988. Entropic elastic processes in protein mechanisms. I. Elastic structure due to an inverse temperature transition and elasticity due to internal chain dynamics. *J. Protein Chem.* 7:1–34.

Walz, T., P. Tiffmann, K. H. Fuchs, D. J. Müller, B. L. Smith, P. Agre, H. Gross, and A. Engel. 1996. Surface topographies at subnanometer resolution reveal asymmetry and sidedness of aquiporin-1. *J. Mol. Biol.* 264:907–918.

Yang, J., J. Mou, J.-Y. Yuan, and Z. Shao. 1996. The effect of deformation on the lateral resolution of atomic force microscopy. *J. Microsc.* 182: 777–785.

Yang, J., L. K. Tamm, A. P. Somlyo, and Z. Shao. 1993a. Promises and problems of biological atomic force microscopy. *J. Microsc.* 171: 183–198.

Yang, J., L. K. Tamm, T. W. Tillack, and Z. Shao. 1993b. A new approach for atomic force microscopy of membrane proteins: the imaging of cholera toxin. *J. Mol. Biol.* 229:286–290.